EUROPEAN ORGANIZATION FOR NUCLEAR RESEARCH

CERN --- AB DEPARTMENT

CERN-AB-Note-2008-057 ATB

EURISOL-DS/TASK2/ TN-02-25-2008-0031

EURISOL-DS Multi-MW Target
Test predictions for the converter target

Karel Samec, Mats Lindroos, Yacine Kadi,
Cyril Kharoua, Roberto Rocca

AB Dept. ATB
European Organization for Nuclear Research (CERN)
CH-1211 Geneva 23, Switzerland

Abstract

The Eurisol project has been initiated by the European Commission to demonstrate the feasibility of a facility for producing large yields of exotic isotopes.

At the core of the projected facility, the neutron source produces spallation neutrons from a proton beam impacting dense liquid metal. The liquid metal circulates at high speed inside the source, a closed vessel with a beam window. The type of the design is diversely described as coaxially guided stream or CGS; an outer annulus converges towards a concave conical shell from which the liquid metal reverses back in the opposite direction.

The current CGS design of the source has been built and is to be tested. This technical report summarises preparations for the test and predictions.

We acknowledge the financial support of the European Commission under the 6th Framework Programme "Research Infrastructure Action- Structuring the European Research Area" EURISOL DS Project Contract no. 515768 RIDS. The EC is not liable for any use that may be made of the information contained herein.

Geneva, Switzerland

16 September, 2008

Table of Contents

-

List of Figures

-

R e f e r e n c e s

-

[Ref1]	K. Samec: Design of the Eurisol converter target		
	TM-34-07-05	PSI Internal Project Note	July.2007
[Ref2]	J. Freibergs: Engineering design and construction of a functional Hg – loop		
		IPUL annual report	April 2008
[Ref3]	Y. Takeda, K. Samec: Experimental measurement of 2Dvelocity vector field using ultrasonic velocity profile monitor (UVP)		
	Vol.128 p47-59	ASME Experimental & Numerical Flow visualization	1991

1 Introduction

The Eurisol converter target CGS scheduled for hydraulic testing at IPUL this year needs to be prepared carefully and any test of the converter target should be preceded by a detailed review of its integration with the IPUL mercury loop.

Safety procedures are mandatory. Indeed, the Eurisol converter target CGS is to be connected to a liquid metal loop operating at high pressure, up to 10 Bar relative and with a mass flow rate of up to 178 kg/s (13 l/s), all of which give rise to concerns about safety.

The design is analysed in its original form as shown in the figure below. There have been modifications since this design was proposed in [Ref1]; the engineering drawings issued by the design office have made changes to facilitate production. However for reasons of expediency these changes may be accounted for in the analysis by scaling the results from the original design manually according to the difference in mean velocity based on the relative section change.

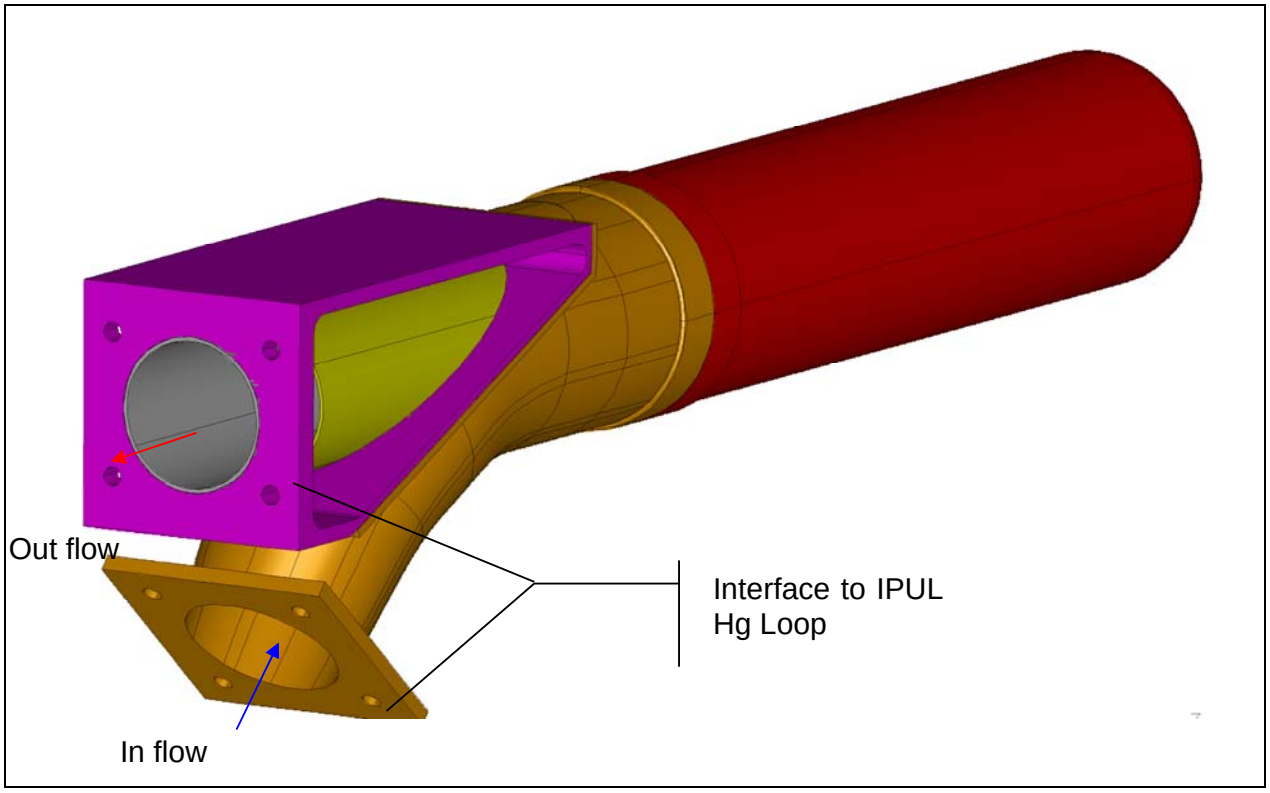

Figure 1: EURISOL Mercury energy converter design [Ref.1]

The base design as described in [Ref.1] is presented below in section for completeness. The section view shows the detail of configuration which will be tested, the most critical area being the forward flow reverser which features some very thin vanes reminiscent of slats on an airplane wing. The reverser is dismountable and the source will be tested in both configurations with and without to better asses the effectiveness of such a design.

Essentially, the liquid metal enters the target from below entering an off-axis diffuser inlet which distributes the fluid into the incomer, an annular-shaped tube between the guide tube and outer hull. At the beam window (right hand cone in the figure below), the liquid metal reverses direction through 180° at a point where it is impacted by the proton beam, it then exits the target down the outflow tube, from which it passes into a separate heat exchanger.

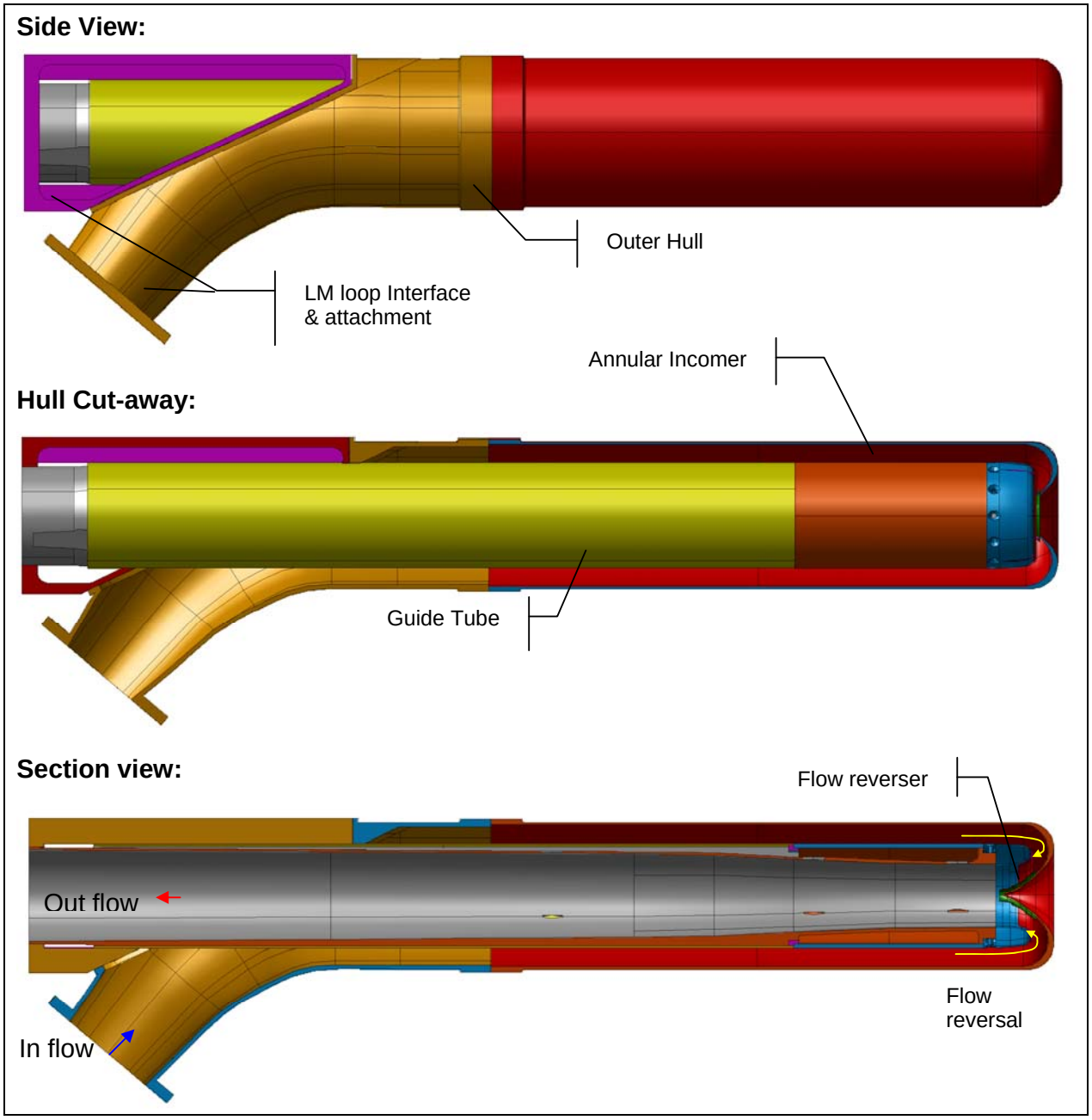

Figure 2: section view showing detail of the structure [Ref.1]

The test scheduled for the end of 2008 is critical to validating a design which has been arrived at using numerical tools only. Most programs involving liquid metal targetry in the past have resorted to extensive testing with water in transparent containers to allow visualisation of the flow.

It is worth mentioning however that this type of window shape was tested with water at PSI in the 1990s [Ref3] as shown in Figure 3 and indicated that a conical pointed beam window would result in a fairly stable flow pattern. The tests carried out at the time also indicated that if the guide tube were a simple cylindrical shape, there would be a recirculation zone behind the guide tube in the outflow region. This problem has been avoided with the design being currently tested thanks to a venturi shape of the guide tube.

In essence, although the usual approach with a water test has been skipped in the current program, there does exist prior experience which indicates that the concave conical shape for the beam window holds promise for current and future developments in high power targetry.

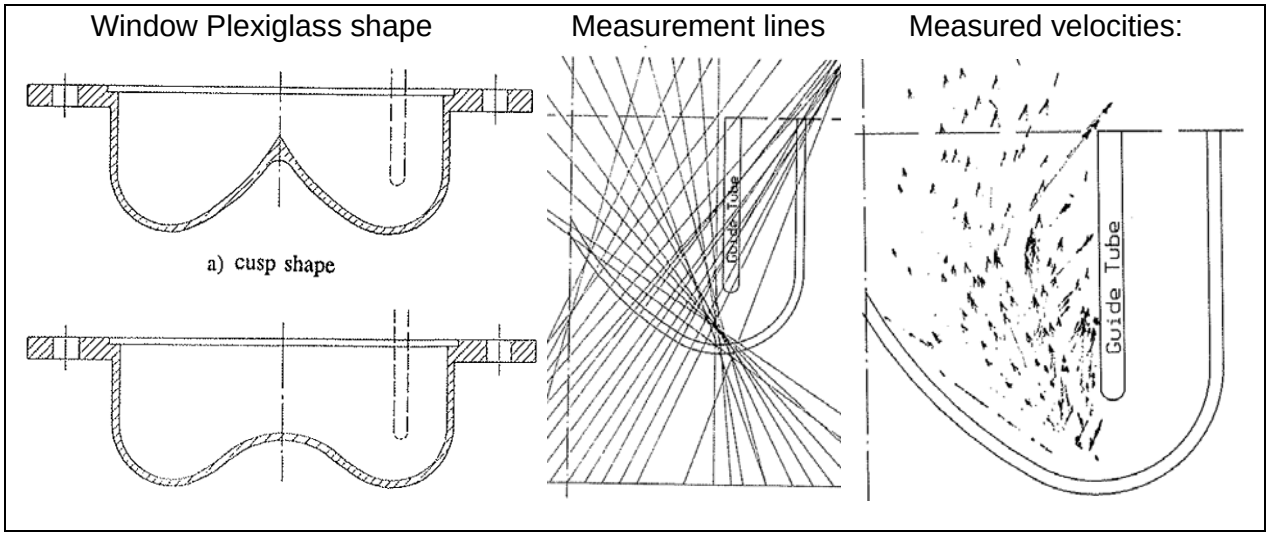

Figure 3: Window cusp-shapes tested at PSI [Ref.3]

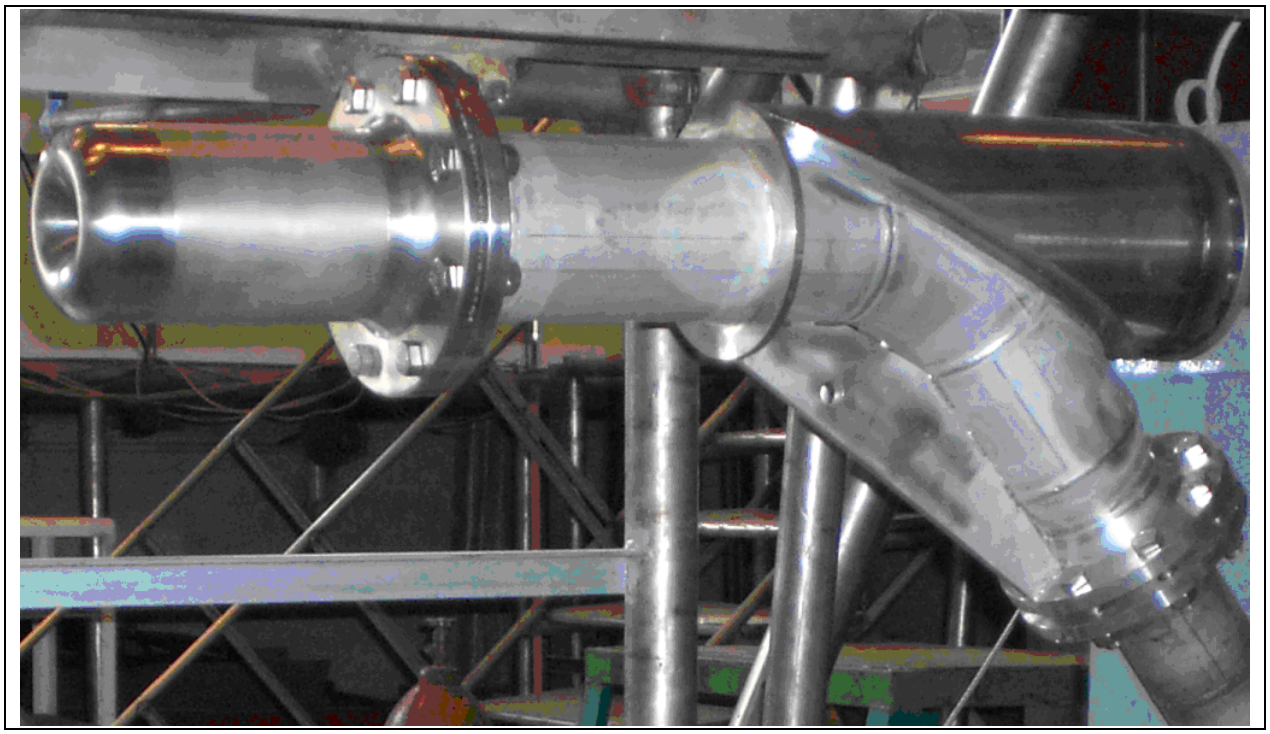

Figure 4: Prototype on test-stand

2 Hydraulic analysis

The use of Computational Fluid Dynamics (CFD) is now quite common to predict liquid metal flow patterns. Prior experience with the Megapie project at PSI as well as experiments such as Achlim at FZK have demonstrated reasonable agreement with the standard turbulence models implemented in commercial codes as for instance CFX which will be used in the following.

The CFD model does not include any structure, nor heat deposition from the beam as it is to be used solely for predicting behaviour in the upcoming hydraulic test. A further development of the model with heat transfer will follow the current hydraulic study at a later stage. The model has 3 million cells. Initially, the turbulence is modelled using an SST (Shear Stress Transfer) model, as it is more stable numerically although it lacks the ability to resolve some periodic turbulent structures which may be of interest. Hence the SST model is only used to ramp up the fluid flow in the target to full power at which point the analysis proceeds with an LES (Large Eddy Simulation) turbulence model, using the results at full power for initial conditions. The ramping up of the flow does however yield interesting information on the pressure drop across the target. The ramp-up function to full power is shown schematically below.

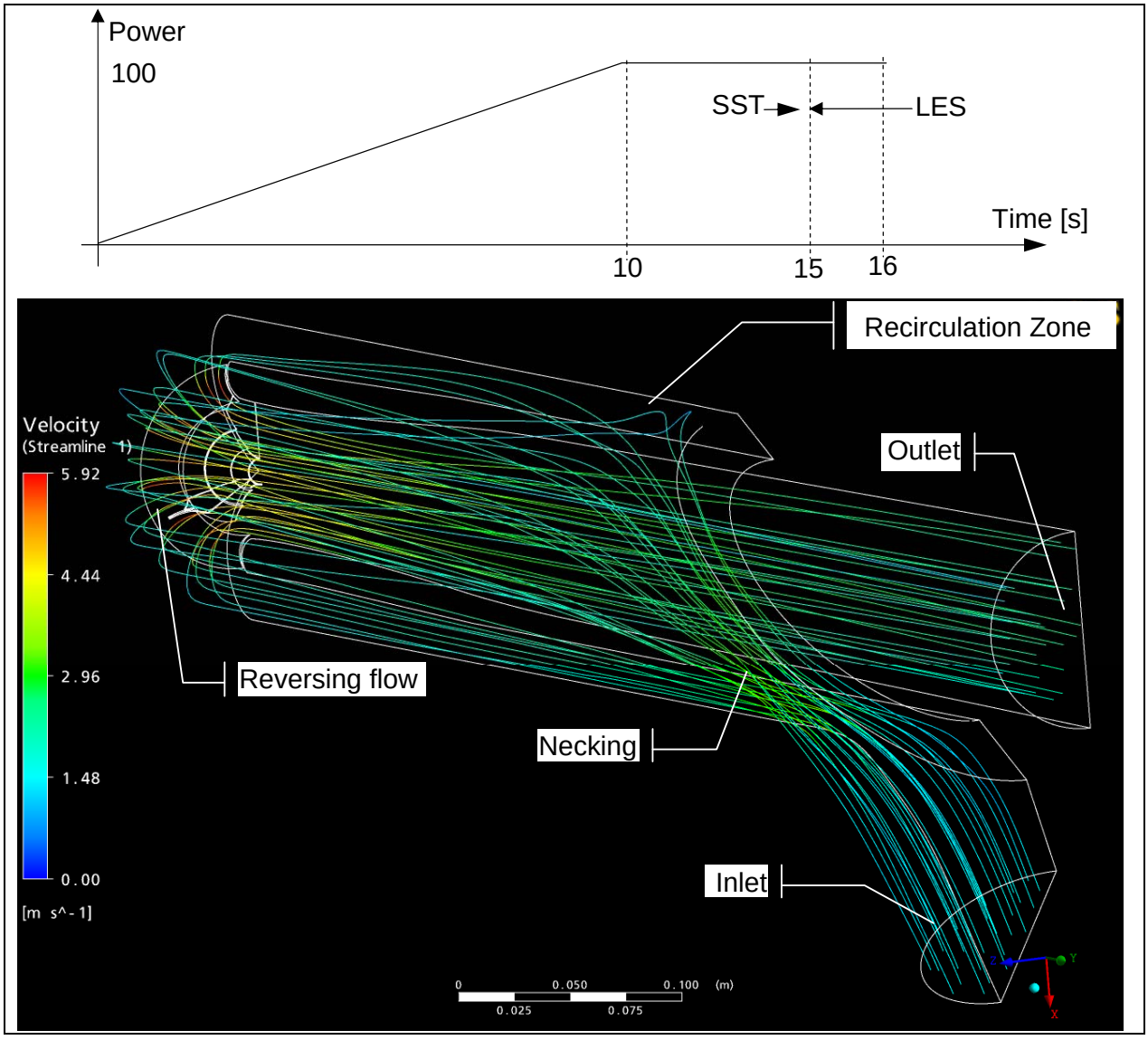

Figure 5: Ramp-up of the flow and flow pattern thru the converter target

2.1 Description of the model

The CFD model of the full target uses half-symmetry through the longitudinal vertical plane, to reduce its size. The reason underlying this model assumption is that any major flow dissymmetry which may occur is more likely to occur between the upper and lower half of the source. The likelihood of a local dissymmetry such as a Von Karman vortex arising behind the support of the vanes is studied by splitting the top support in half, which results in one of the supports being at 120°, totally surrounded on either side by fluid.

The three-dimensional CFD model is highly complex and encompasses three million cells in a structured hexahedral mesh. The figure below shows model details areas of particular interest such as around the vane supports, the vanes proper and the inner surface of the beam window.

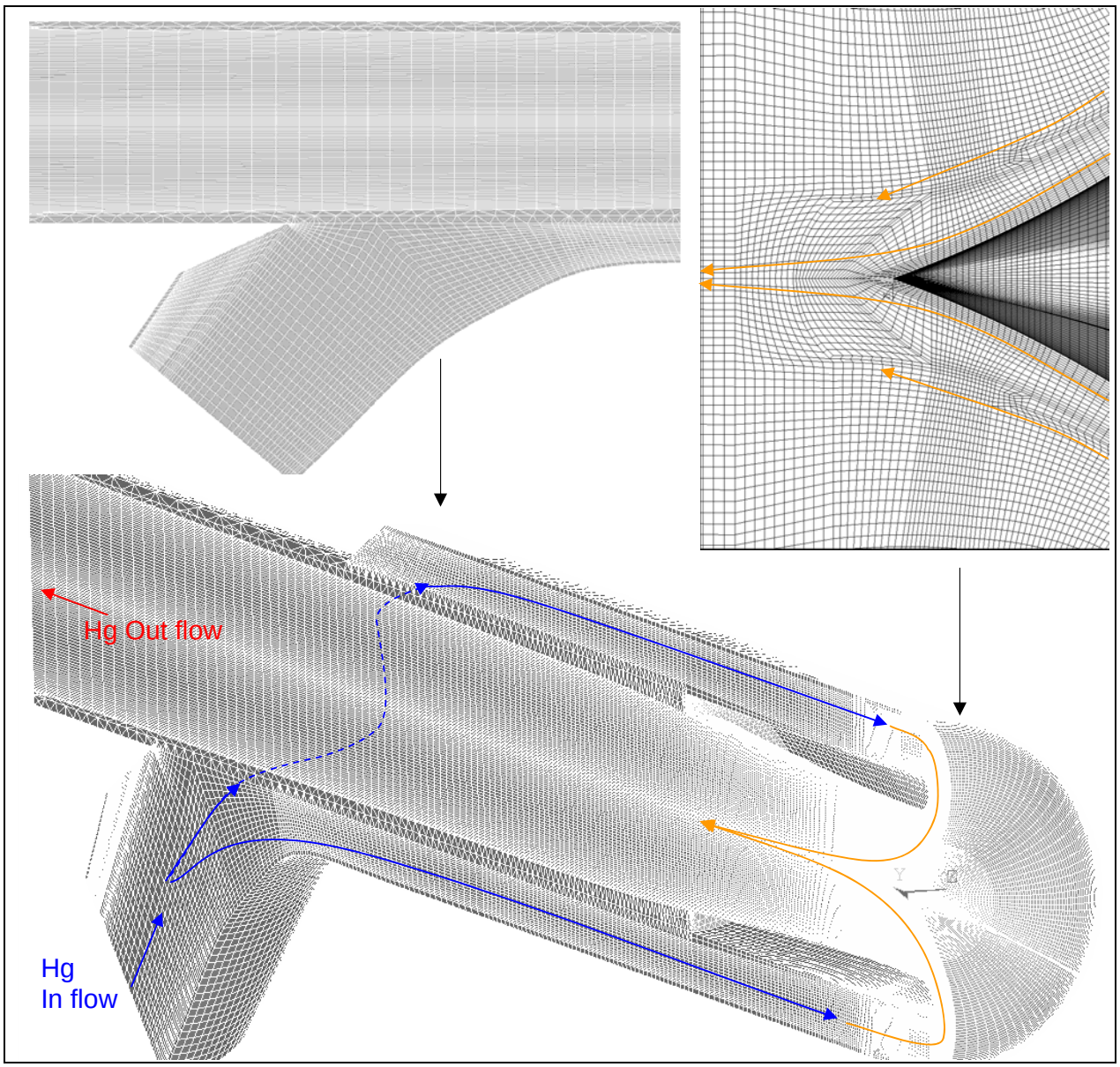

Figure 6: CFD Model details

The physical models for the fluid are strictly limited to the requirements necessary for predicting hydraulic behaviour in the most effective manner. This entails in particular that the following restrictions apply;

- There is symmetry in the vertical plane.
- The inlet turbulence is 5%
- The outlet pressure is defined at 0 Bar relative and defined as an opening (which allows two way flow)
- The fluid is one phase and non buoyant
- There is no transfer of heat to the wall nor heat deposition from the beam
- The SST model is used to ramp up the fluid flow to nominal (178 kg/s) over 10 seconds.
- The LES turbulence takes over after a 5 second stabilisation and is run for at least 1 second

2.2 Pressure losses in the source

The pressure losses from inlet to outlet are shown in Figure 7, and are well below 1 Bar which is within the systems specification set out early on in the program. The areas in blue at or below -1Bar relative, or 0 [Bar] absolute indicate that cavitation will occur locally unless the static pressure in the loop is increased. A detail look at the structure of the pressure contours around the vanes indicates that an overpressure is required to suppress cavitation locally around the forward end

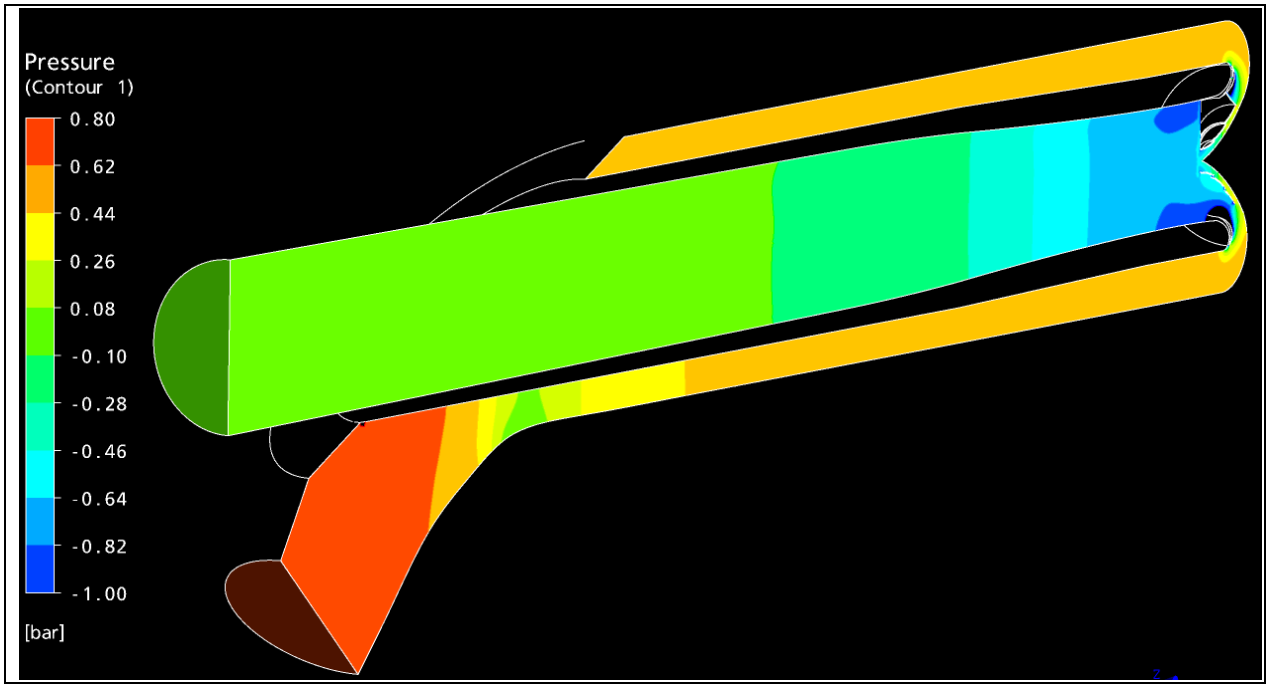

Figure 7: Static pressure distribution at 100% nominal flow (178 kg/s) on the model with vanes

Reference pressure: 0 Bar at outlet

The pressure losses increase gradually along the duct as expected due to friction on the walls. There are some inertia effects as well to consider when accelerating the fluid which is initially at rest. This may influence results somewhat during the ramp-up to full power. The pressure losses i.e. the pressure difference between inlet and outlet increases with the square power of the flow rate. There is some numerical instability on this pressure curve due the inertia, but overall the power law hold true, and the instabilities can easily be filtered out.

The outlet pressure is fixed at 0 Bar, so all static pressures in the conduit are relative to this reference static pressure. In the test the actual static pressure will be varied between 3 to 5 Bar currently. Results from the ramp-up to full power using the SST model show the dependence between pressure drop across the target and flow rate follows a square law (Figure 8,top).

The pressure drop is recorded in the simulation as the difference between the average outlet and inlet pressure. The pressure drop at full power satisfies the overall system requirements. This experimental parameter will be measured in the coming test and may serve as a fair indication of the validity of the models used in the hydraulic design.

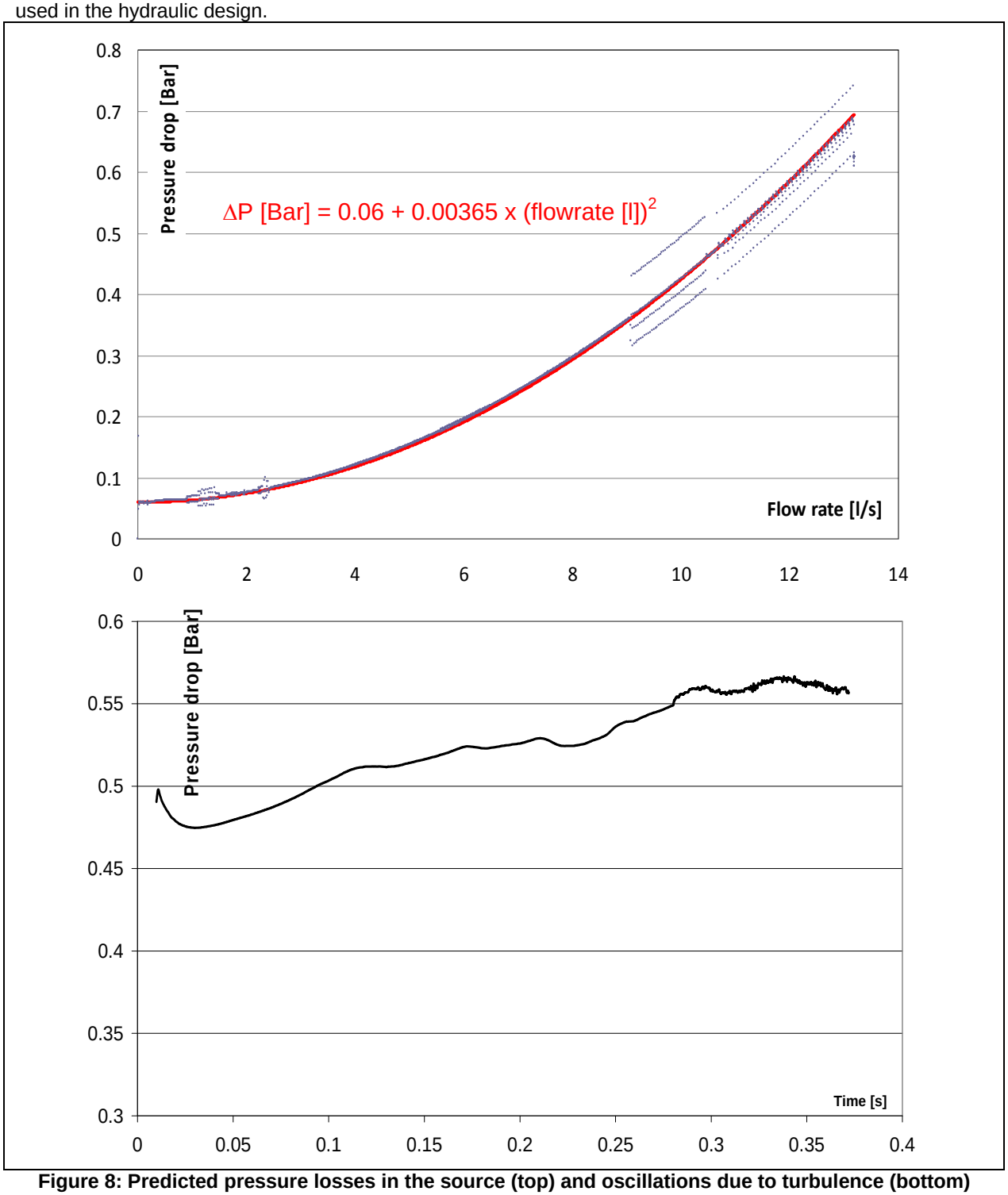

Figure 8: Predicted pressure losses in the source (top) and oscillations due to turbulence (bottom)

The boundary conditions specify a fixed entrance mass flow rate, and zero relative pressure at the outlet. Therefore, at each step of the calculation, the CFD will balance the inertial forces of the fluid with these imposed external boundary conditions. Recording the inlet/outlet pressure difference during the LES simulation (Figure 8,bottom) is therefore an indication not only of the pressure losses due to friction, but also serves as an indication of the stability in the flow.

As indicated previously the ramp-up function of the flow during the initial SST run does produce inertial forces in the fluid which, if the ramp is too steep, will cause in numerical instabilities which are not realistic The LES pressure drop initially declines and then increases until a plateau is reached at which point the pressure drop seems to settle back to the original value calculated with the SST model. Bar a few high-frequency oscillations there does not appear to be any major oscillatory movement in the fluid, as is borne out by observing the velocity field; refer to figures hereafter which show the velocity field in the vertical symmetry plane, and in sections taken at 10 cm intervals down the axis.

The rather complex flow pattern resulting from this configuration is necessary to evacuate the heat deposited both in the liquid metal but also in the conical beam window. It is feared that instabilities may arise at the tip of the conical beam window where the beam deposition is highest.

Two different configurations have therefore been proposed. The more advanced configuration features a series of hydro-dynamically optimised vanes, called a flow reverser, shown in Figure 9 below, aimed at “combing” the fluid as it reverses back into the outflow tube; it should also ensure stable rapid flow along the beam window.

A design option without these vanes is also being envisaged. Both configurations are to be validated experimentally in a dedicated full-scale test, and have therefore been investigated ahead of the test with CFD, in particular with an LES turbulence model which is most adapted to studying large-scale oscillatory turbulent phenomena.

The design shown on the left side of Figure 9 is rather complex to manufacture, and it is one of the goals of the test to determine it’s degree of effectiveness. The velocities taken along various longitudinal sections are shown on the right of the figure and indicate quite clearly an area of high acceleration at the beam window, where the vanes have been located.

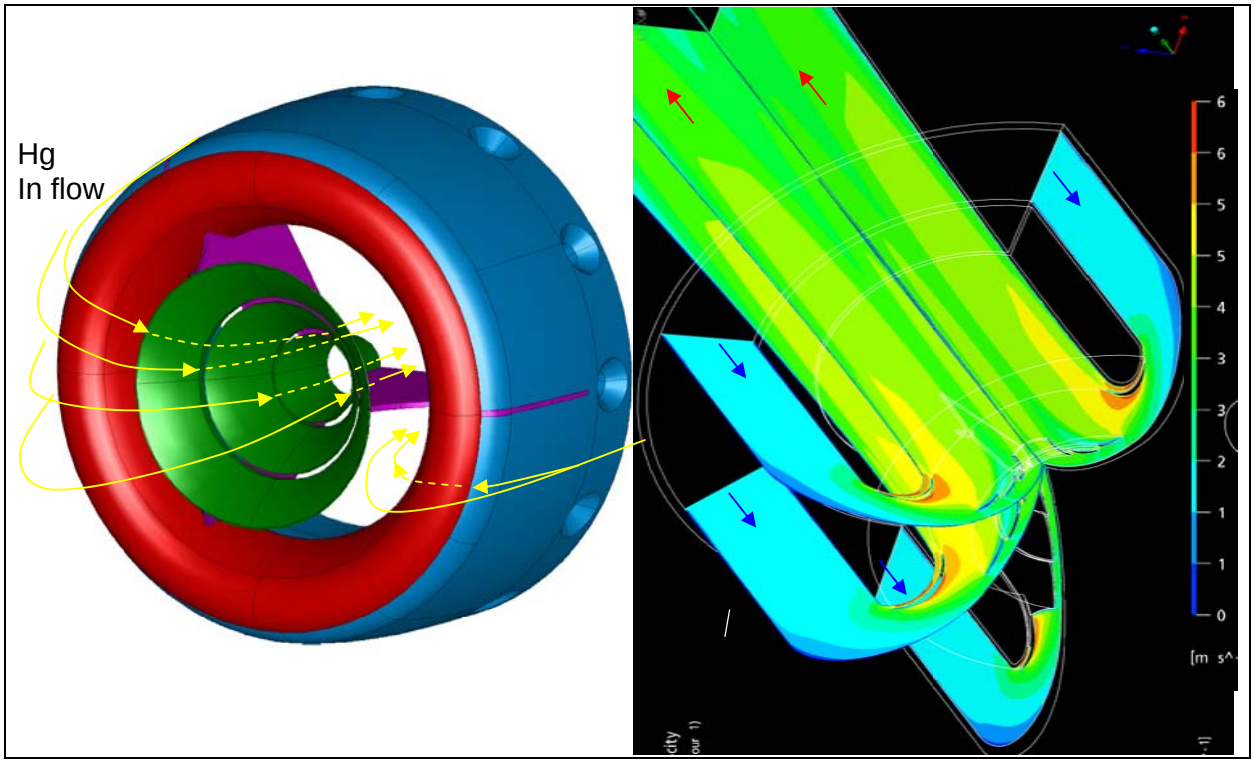

Figure 9: Flow reverser design (left). Detail of the beam window flow pattern and velocities (right)

2.3 Instabilities in the flow

The velocity field during the LES simulation indicates a steady flow configuration over the window with the flow reverser but an oscillating detachment if the reverser is omitted. The structure in the outflow channel is also more unsteady without the flow reverser.

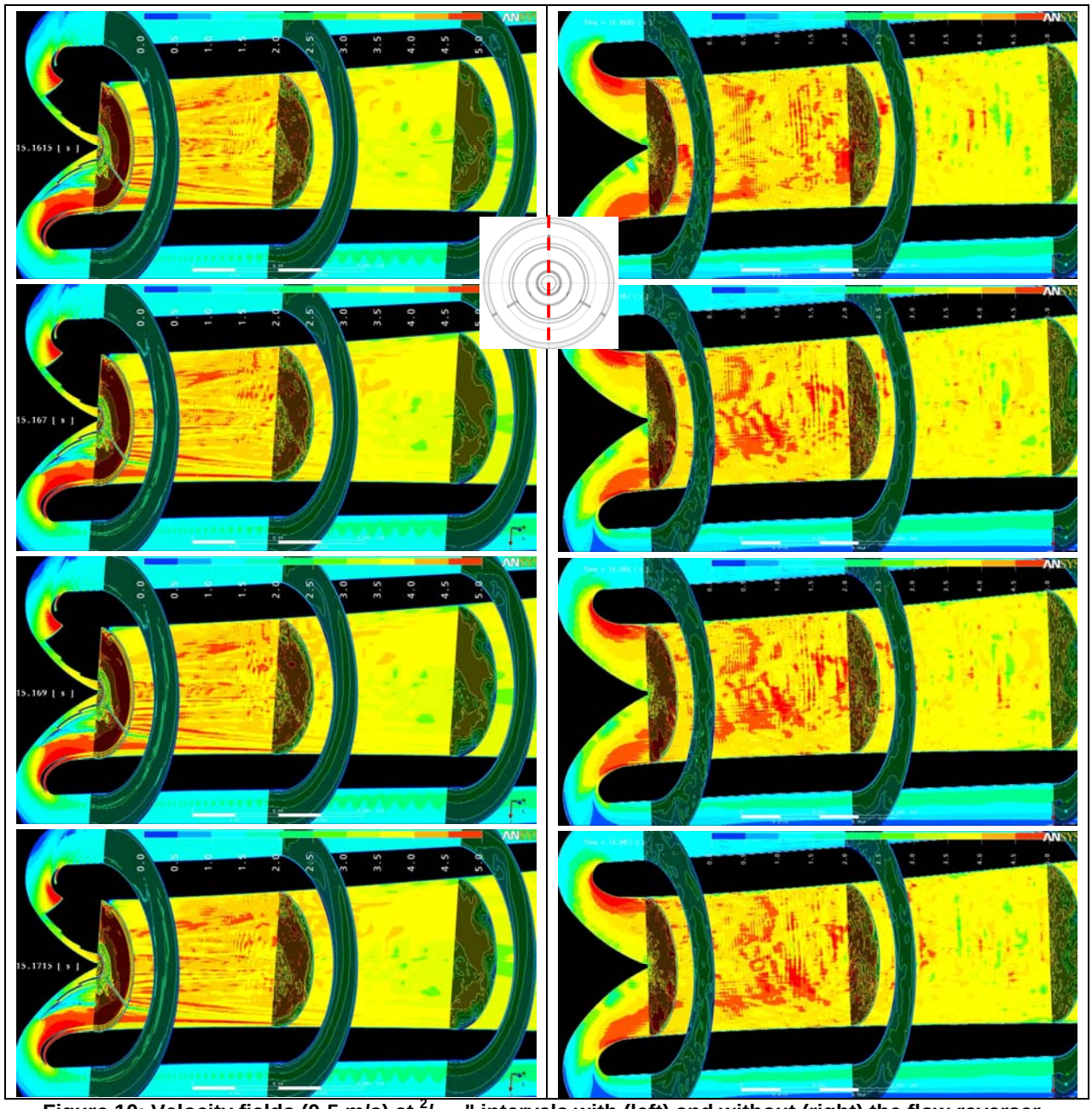

Figure 10: Velocity fields (0-5 m/s) at $^{2}/_{1000}$" intervals with (left) and without (right) the flow reverser

The pressure fluctuations from the large-scale instabilities are limited to the inner surface of the guide tube which is therefore more likely to be subjected to vibrations than the outer shell, where the velocity is both smaller and appears more stable.

The beneficial effect of the reverser seems therefore to be both in terms of limiting vibrations in the outflow and precluding cooling variations on the beam window which would have a detrimental effect on the lifetime through high cycle fatigue.

2.4 Cavitation

Cavitation does tend to occur at a lower pressure with the reverser in place due to high local velocities around the vanes. This effect may be combated by adjusting the static pressure accordingly, at the following values:

- Without blades: +1 Bar
- With blades: +2.6 Bar

3 Stress analysis

The current stress analysis of the converter target focuses on the outer hull which is structurally the main load-bearing component, and for which a simplified FEM shell model is set up.

3.1 Pressure case

The maximum static pressure applied to the inner surface of the converter target is 10 bar, with local variations around this value due to the circulation of mercury at high speed. However as far as the stresses in the most critical parts is concerned, the 10 bar pressure case is dimensioning.

$$\Delta P = 10^6 N/m^2 = 1[N/mm^2]$$

The resulting stress distribution in the converter target outer hull is shown in the figure below. There is a concentration of bending stresses in the cusp region of the window due to the pressure being reacted by the apex of the window which in turn pushes on the inner rim on the cusp and tends to push it inside-out. These stresses are fairly low, and do not act in conjunction with other peak stresses in the hydraulic test. The allowable design stress at temperatures below 100°C is 400 [MPa] for T91. Hence the safety margin against ultimate failure (S.F. = 1.5) is,

M.o.S. = 400 / (1.5 ^{x} 79.6) -1 = 2.3 against ultimate pressure failure at 10 Bar

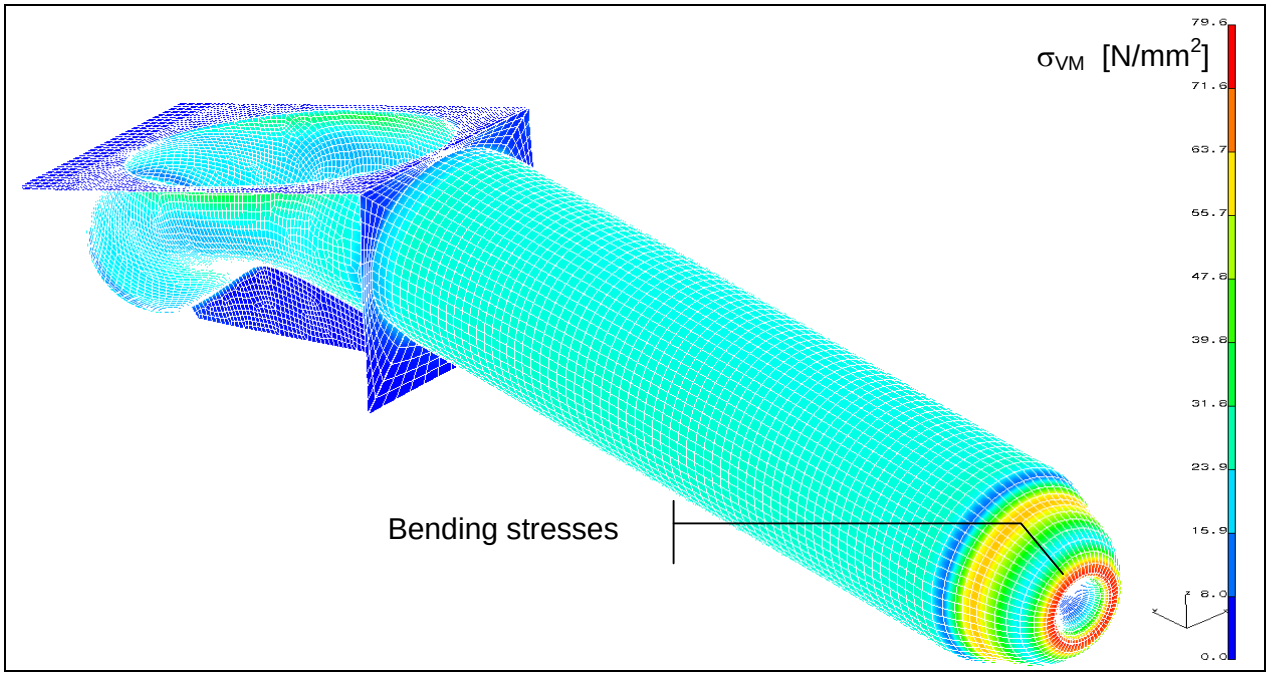

Figure 11: 10 Bar Pressure case Von Mises stress distribution

Furthermore it should be emphasised that under operational conditions, pressure stresses will add to the concentration produced by the beam, however satisfactory safety margins have already been demonstrated in the Eurisol design study for this particular case.

3.2 Resonance case

The very high velocities in the liquid metal may cause natural resonance modes in the structure to be activated, which in turn could lead to excessive stresses in the outer hull. In order to gauge the magnitude of this potential problem, a first order approach is to simply add the entire mass of liquid metal to the outer structure and calculate the Eigen-frequencies using the FEM Lanczos method.

In actual fact, any disturbance in the flow coming from the inlet will propagate down the annulus towards the window, and it is only this mass of liquid entering the target which will participate in the postulated coupled resonance phenomena. So by adding all the mass in the target to the mass of the hull, the calculated value of the first Eigen-frequency will probably be lower that in reality. However it is the lowest frequencies which are the most likely to damage a structure, as such the approach is conservative.

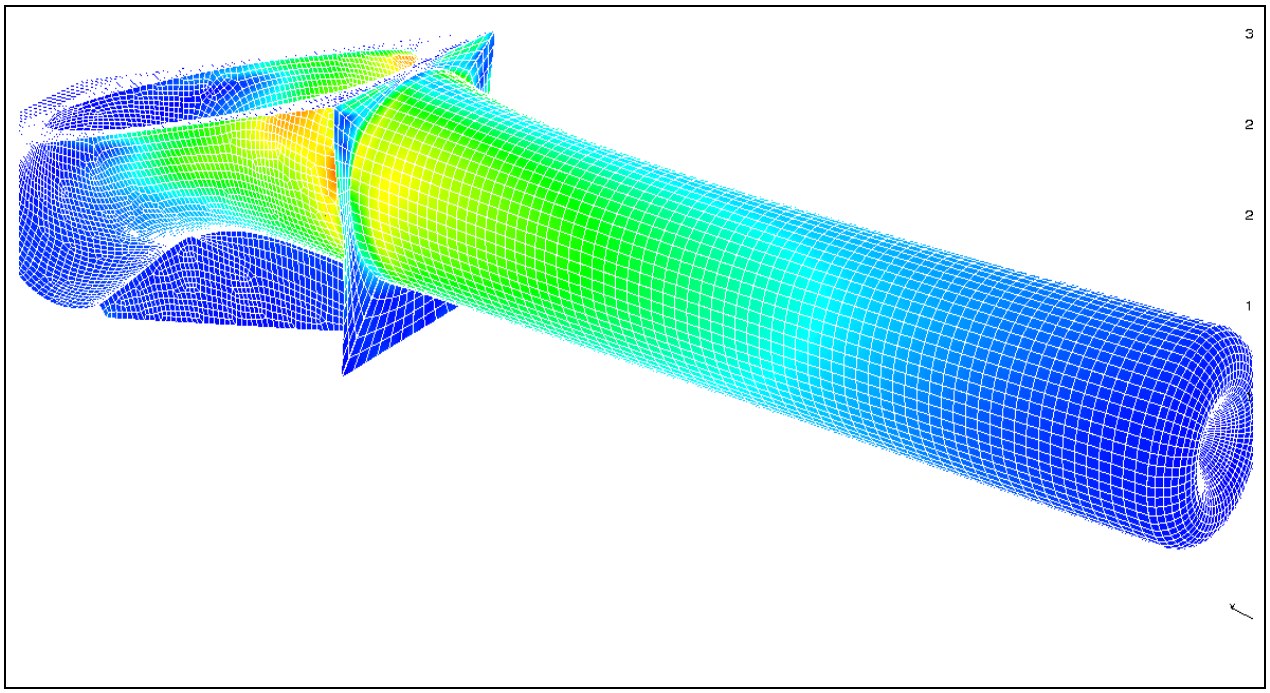

Figure 12: Mode shape and Von Mises stress in the first Eigen mode at 62.2 Hz. Lateral vibration.

The stresses shown in figures 11 and 12 above have been calculated for a normalised Eigen-frequency vector. There are an infinite number of solution displacement vectors since the analytical method derives the mode shapes from a diagonalisation of the stiffness matrix. The stresses shown in the figures correspond to very large displacements for a mass-normalised Eigen-vector, which is physically impossible. To continue with this method, a full dynamic analysis is needed, which entails applying a PSD function of the excitation load to the wetted walls of the structure, calculated from the fluid turbulence.

Rather than engage in such a dynamic analysis, it is easier to calculate stresses from an enforced static displacement which results in roughly the same structural deformations as the characteristic Eigen-mode shape. The first mode shown in figure 12 indicates that the stresses are caused by a lateral bending of the outer shell. In the corresponding static stress case shown in Figure 14, the entire window is shifted 1 mm to the side and stresses are calculated accordingly. This gives a fair assessment of the structural limits the hull may endure without failure.

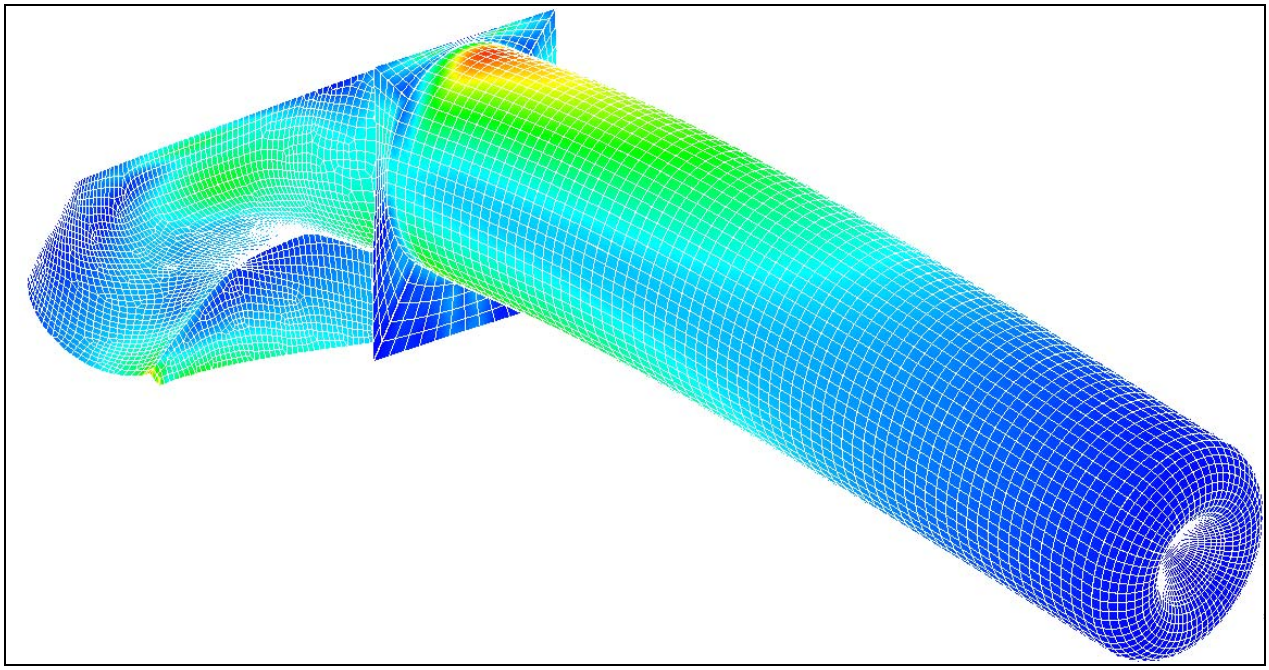

Figure 13: Mass-normalised Von Mises stress in the second vertical Eigen mode at 67.8 Hz.

3.3 Lateral displacement, 1 mm

A 1 mm lateral displacement is enforced at the window. Results below show the stress pattern is quite similar to that obtained in the resonance case for the first Eigen-mode.

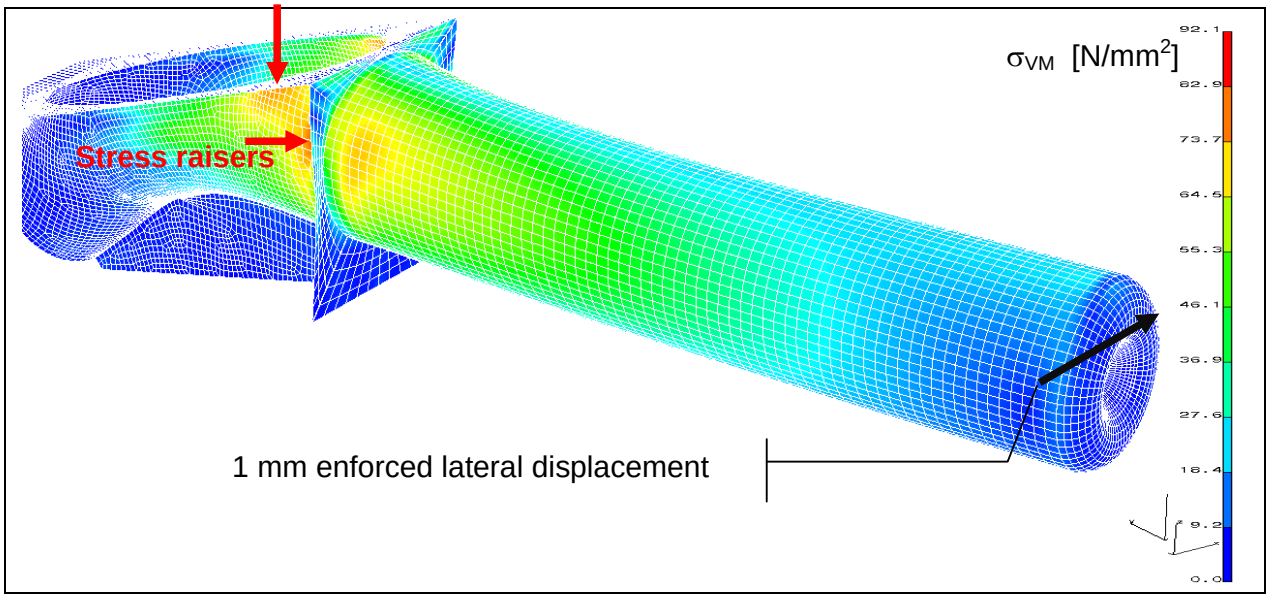

Figure 14: Von Mises stress distribution for the 1mm Lateral displacement case

The stress peaks visible in figure 14 above are unfortunately located close to weld seams which have to be examined in more detail. Since the FEM consists in 2D shell elements, the best method is to extract the element shell stresses in critical areas indicated by the arrows in figure 14 above. The relevant plate elements

are chosen according to their position with respect to the stress peaks and weld locations. This is illustrated in the next few figures by a comparison of a side view of the inlet tube with the stress distribution.

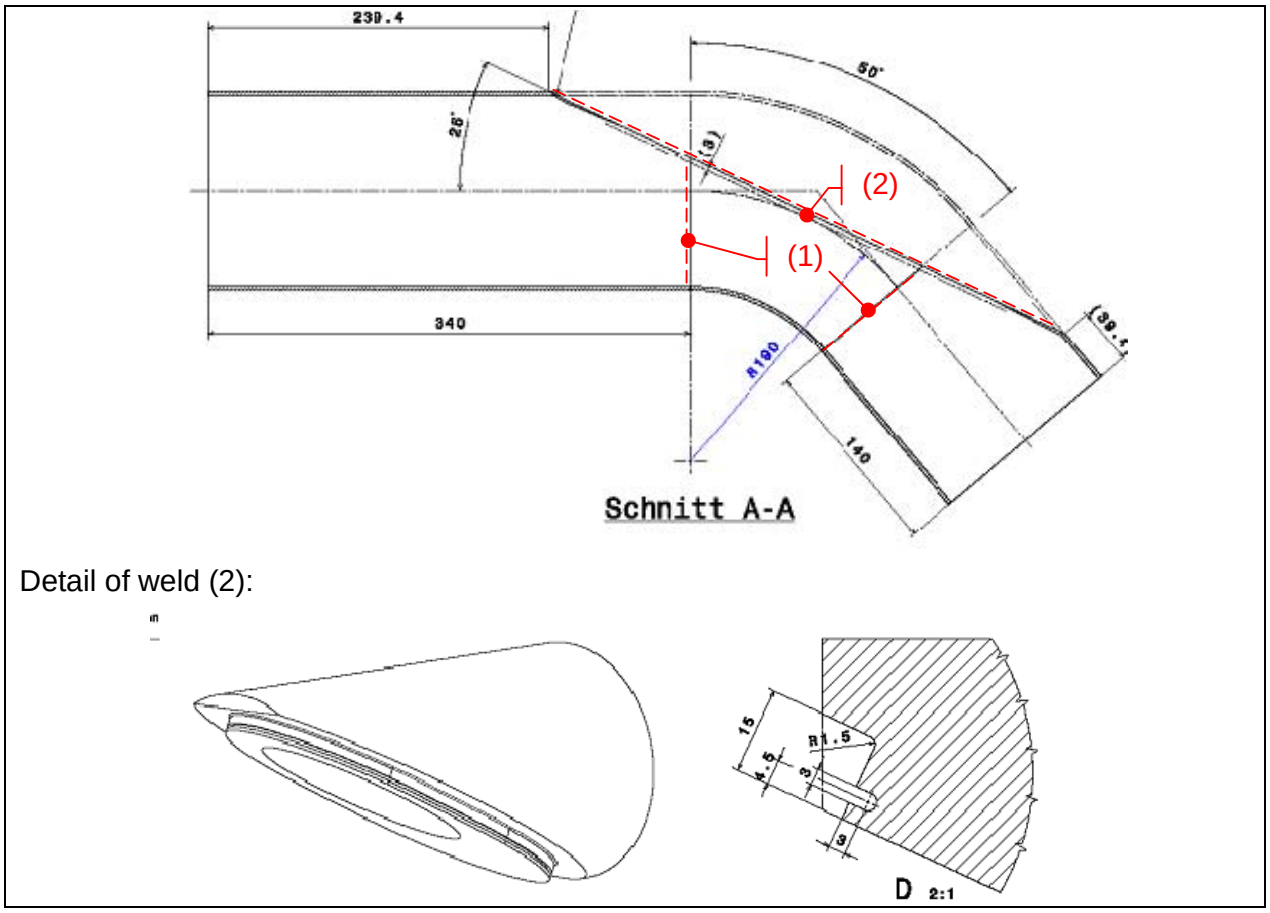

Figure 15: Detail of the welds in the inlet tube

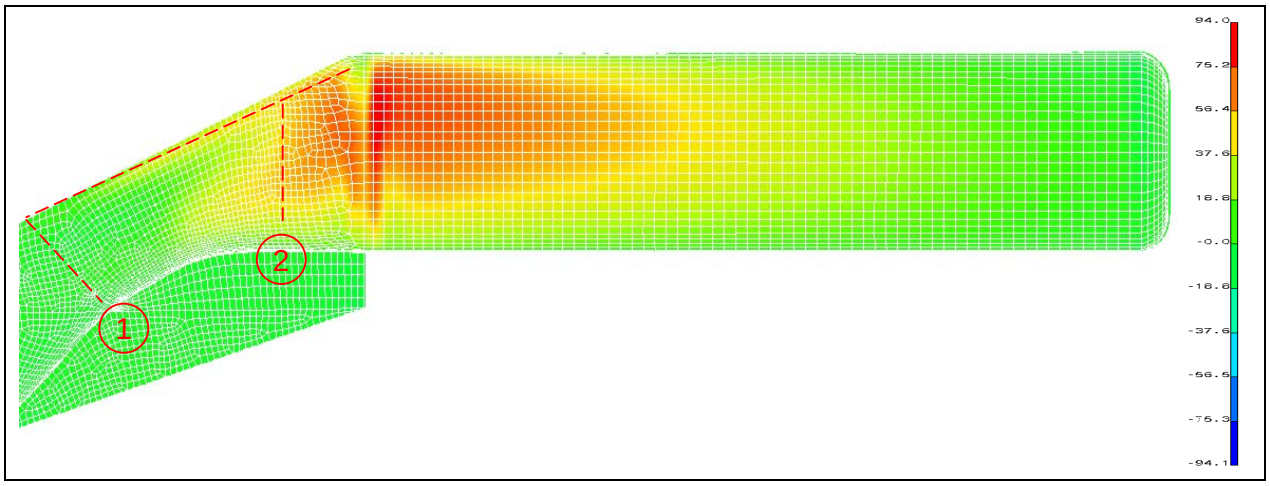

Figure 16: Stress distribution in global longitudinal direction for the 1mm Lateral displacement case.

There are fundamentally two types of welds at risk: The first (1) in figure 16 is a conventional V-weld around the perimeter of the tube either end of the bend, the second (2) is a weld to a scarf-type junction running the full perimeter of the angled cut where it joins onto the fixture for holding the target to the test rig.

The stresses in longitudinal direction are shown in figure 16 above and reach a peak of 95 [N/mm^2] for a 1 mm lateral enforced displacement. In the vicinity of weld 1, longitudinal peak stresses are in the order of 70 [N/mm^2]. As this is a V-weld (Stumpfnaht) the section need not be reduced other than by the weld factor (Schweissfaktor). For a qualified welder (SVTI geprüft) this factor is 0.8. Hence the margin on weld 1 is;

M.o.S. = 0.8 ^{x} 400/ (1.5 ^{x} 70.0) -1 = 2.05 against ultimate failure of weld N°1 for a 1mm lateral displacement of the window

For the second weld (2 in figure 6 and 7), the stress is somewhat more complex as the design in figure 15 includes a groove to relieve built-in stresses from the welding of the inlet tube to the fixture. Hence when the lip of the groove is pulled, this will create a stress concentration in the radius of the groove

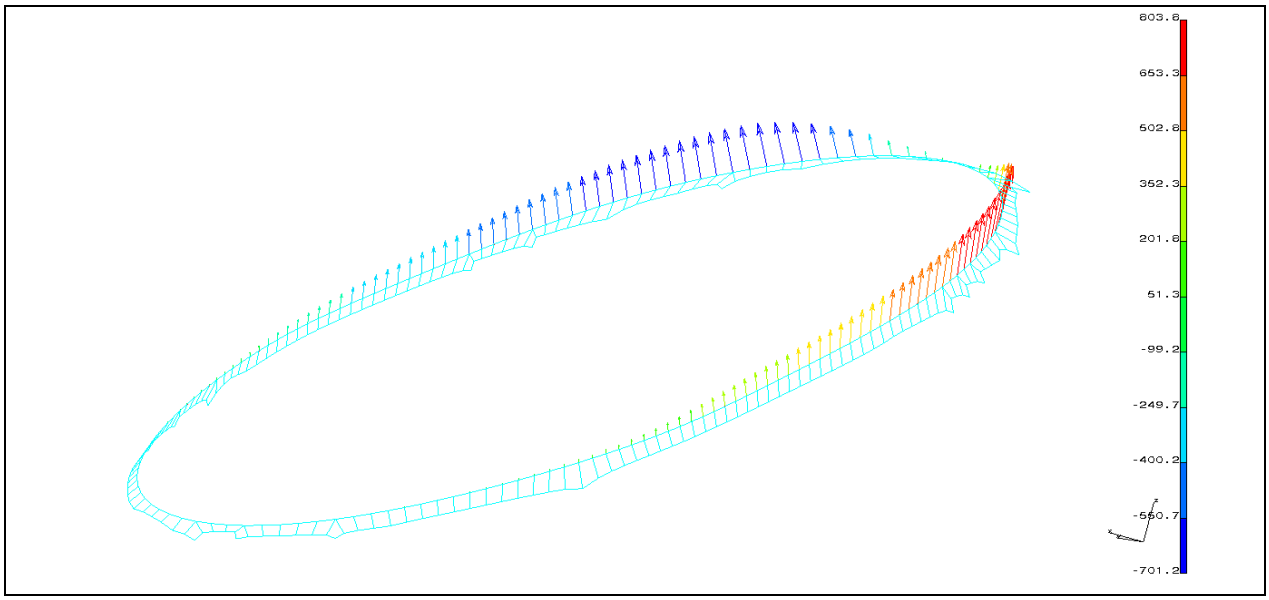

Figure 17: Interface loads at inlet tube interface for the 1mm Lateral displacement case (top)

The underlying assumption in the model is that the tube is connected edge-on to the interface. In reality there is a weld seam along the face which displaces the line -of-action of the and tends to open the groove more . It is therefore more relevant to determine the stress at the location indicated by 2 in figure 15, but at right angle to the weld, not in the global longitudinal direction. This may easily be derived from the reaction load at the nodes where the inlet tube attaches to the slanted scarf as pictured in figure 17. The magnitude of the nodal forces are shown in [N] and can be converted to a running load by dividing the average pull-out component of the nodal forces by the average distance between nodes.

$f = \Delta F / \Delta l = 375 / 5.2 = 72$ [N/mm]

Hence the revised stress concentration in the groove can be obtained from the classic formula:

$\sigma = 6 \times (M/f) / t$

Where :

t is the thickness of the weakest section = 3 [mm] (see fig.6)

(M/f) is the running bending moment in Nmm /mm $= f \times b$

and b is the moment arm = 2 [mm] (see fig.8)

Hence :

$\sigma = 6 \times (72 \times 2) / 3 = 288$ [N/mm2]

This will yield a slightly negative margin;

M.o.S. = 400/ (1.5 x 288) -1 = -0.07 against ultimate failure of weld N°2 for a 1mm lateral displacement of the window

Weld 2 is clearly a weak point in the structure which has to be monitored carefully. It is difficult to reinforce the structure at such short notice, so the best option is to install a strain gauge close to the weld. For zero margin the lateral displacement must be no more than:

$\Delta x = 1$ mm x 400/ (1.5 x 288.0) = 0.92 [mm]

This corresponds to a lateral acceleration on the window of;

$$\ddot{x} = \Delta x \cdot \omega_0^{\,2} = \Delta x \cdot \left(2\pi f_0\right)^2$$

where; f_0 = 62 [Hz] estimate of first lateral eigenfrequency, which results in the following limit for the lateral acceleration, as

$$\ddot{x} = 139\left[m/s^2\right] = 14\,[g]$$

However the acceleration limit depends critically on the Eigen frequency and the resonance phenomenon depends on the amount of entrained fluid inside the target which is difficult to predict. If the real structure resonates at a lower frequency, the acceleration limit at which damage occurs will be much lower, hence under-estimating the Eigen frequency could be dangerous. In reality resonance seldom yields a singular value but rather a continuous spectrum, which makes a derivation of the stress level in the weld from the acceleration rather hazardous.

4 Testing

In light of the observations made above, it is highly recommended the stress level close to the welds be monitored at all times. The stress level for a 1 mm enforced lateral displacement shown in figure 16 is 70 MPa close to the weld and 94 MPa at the most highly stressed area in the tube. By applying the same ratio to the stress level as to the displacement to obtain zero margin on the weld, it is possible to specify a stress limit on specific strain gauge locations to protect weld 2 from ultimate failure.

Stress limit on Strain Gauge Type 1 : 0.92^{x} 94 = 87 [N/mm^2]

Stress limit on Strain Gauge Type 2 : 0.92^{x} 70 = 65 [N/mm^2]

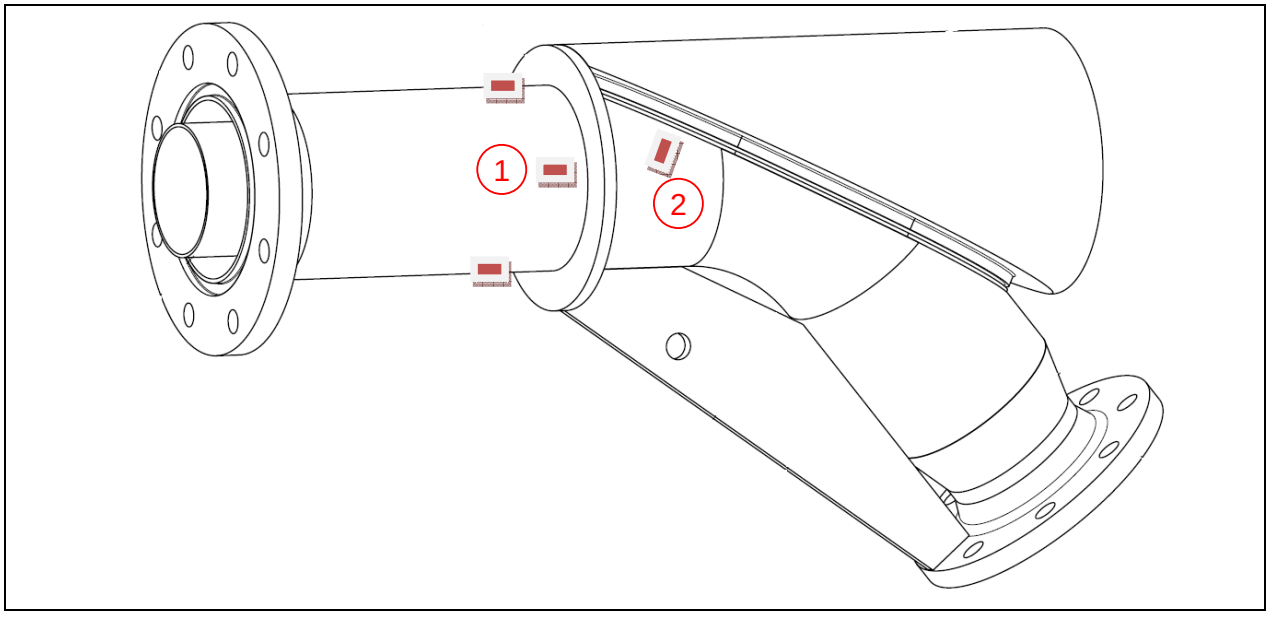

Figure 18: Positioning of strain gauges on the inlet tube

The most likely cause of failure would be coupled vibration between the eigenfrequency of the structure and the turbulence in the running liquid metal. Hence two sets of strain gauges have been set up as shown symbolically above by the type 1 and type 2 gauges.The type 1 gauges are positionned in four different positions, spaced out at 90° around the circumference of the tube so as to pick up bending about either of the two main bending axes. Strain gauges on opposite sides of the tube should be set up in a Wheatstone bridge as a tension/compression couple so as to increase the strengtgh an accuracy of the signal.

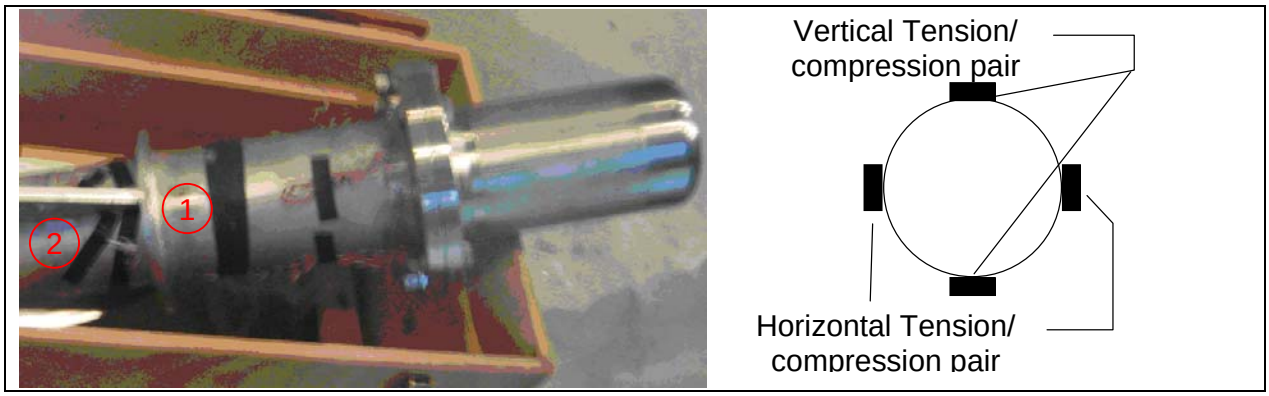

Figure 19: Location of tension/compression strain gauge couples of type 1

As the type 1 gauges are spaced out to pick up vibrations in both horizontal and vertical planes, setting up a data acquisition as a tension/compression couple using a half wheatstoin bridge results in no loss of data. On the other hand, te type 2 gauges should each be aquired seprately by a classical full wheatstone bridge arrangement. Indeed bending in vertical direction would produce in-phase oscillations in these strain gauges, whereas a bending ithe horizontal plane would cause the two type 2 gauges to be 180° out of phase. It would therefore be impossible to distinguish the two main bending modes if the type 2 gauges were set up as a tension/compression pair.

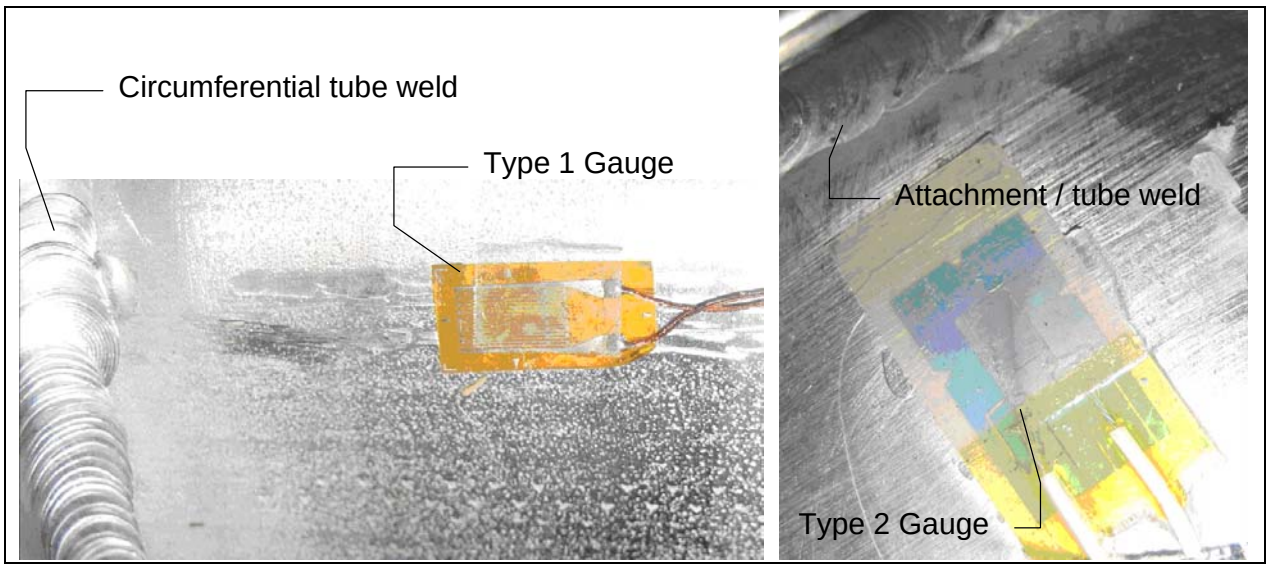

Figure 20: Close-ups of Type 1 (left) and Type 2 (right) strain gauges

The data aquisition system is a poven Spider8 device such as has already been used for the MTR-I3 program sponsored by the EU (figure 21). The oscillation shown on the right side is the measurement result of coupling two strain gauges fixed either side of the test piece in tension/compression using a half wheatstone bridge.

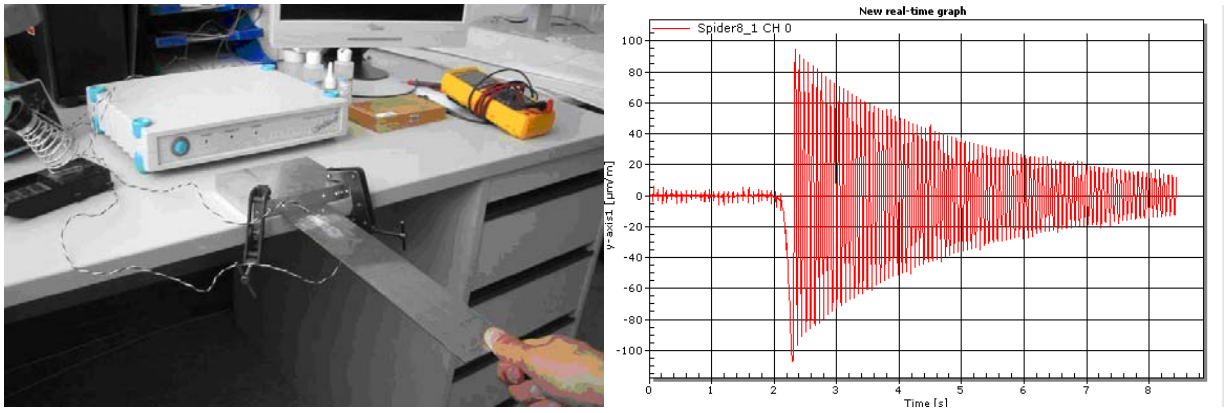

Figure 21: Output from a sample resonance test using standard strain gauges coupled in tension/compression tandem in a Wheatstone bridge

All the gauges have been tested on-site during the safety visit of the IPUL lab on October 17th 2008 and verify the nominal resistance value of 350 Ω. Spares have been set aside.

5 Conclusions

The current work focuses on the hydraulics necessary for the test. There needs to be some additional investigation as to the effect of the pressure fields calculated in the current work on the structure as vibrations may appear due to the strong turbulence in the liquid metal flow.

Two approaches are possible. One is to carry out testing gradually, by ramping up the flow to full power very slowly; monitoring the strain gauges at all times to ensure they are not exceeding the values calculated in this report.

Another, more cautious method providing a better understanding of the test is to apply the varying pressure fields calculated in this work to a structural model of the source in order to derive time-dependent stress predictions at critical locations.

Were the first approach to be adopted, strain gauge monitoring would be a vital necessity at all times as well as an accurate control of the loop in regard to static pressure and flow rate.